

# L- and U-Band WDM Transmission Over 6 THz Using PPLN-Based Optical Parametric Amplification and Wavelength-Band Conversion

Shimpei Shimizu <sup>1</sup>, Member, IEEE, Takayuki Kobayashi <sup>2</sup>, Member, IEEE, Akira Kawai <sup>3</sup>, Member, IEEE, Takushi Kazama <sup>4</sup>, Masanori Nakamura <sup>5</sup>, Member, IEEE, Koji Enbutsu <sup>6</sup>, Takahiro Kashiwazaki <sup>7</sup>, Masashi Abe <sup>8</sup>, Takeshi Umeki <sup>9</sup>, Member, IEEE, Yutaka Miyamoto, Member, IEEE, Tomoyuki Kato <sup>10</sup>, Member, IEEE, Yu Tanaka, Member, IEEE, and Takeshi Hoshida <sup>11</sup>, Senior Member, IEEE

**Abstract**—We demonstrate a 38.4-Tbps (60 ch.  $\times$  640 Gbps) wavelength-division multiplexing (WDM) transmission across 5  $\times$  80-km G.654.E single-mode fibers over 6 THz within L- and U-bands. The U-band (1625–1675 nm) is promising as a next transmission band for multiband networks because of its low transmission loss compared with E- and O-bands, but there are few demonstrations of coherent WDM transmission with the U-band. One reason is that promising optical components, especially for optical transceivers, are underdeveloped for the U-band. An optical parametric amplifier (OPA) using a periodically poled LiNbO<sub>3</sub> (PPLN) waveguide has wide-gain bandwidth and wavelength conversion function, which allows the use of commercially available optical components for new bands. We achieve L- and U-band digital coherent WDM transmission within 1597.2–1649.9 nm (181.7–187.7 THz) using PPLN-based optical parametric inline amplification and wavelength-band conversion.

**Index Terms**—Optical fiber communication, optical parametric amplification, optical wavelength conversion, wavelength division multiplexing.

## I. INTRODUCTION

MULTIBAND wavelength-division multiplexing (WDM) technologies can drastically increase the throughput of

Manuscript received 10 July 2023; revised 4 September 2023 and 29 September 2023; accepted 4 October 2023. Date of publication 9 October 2023; date of current version 4 March 2024. This work was supported by the National Institute of Information and Communications Technology (NICT) of Japan under Grant 04501. (Corresponding author: Shimpei Shimizu.)

Shimpei Shimizu, Takayuki Kobayashi, Akira Kawai, Masanori Nakamura, and Yutaka Miyamoto are with the NTT Network Innovation Laboratories, NTT Corporation, Yokosuka 239-0847, Japan (e-mail: shimpei.shimizu@ntt.com; tkyk.kobayashi@ntt.com; akira.kawai@ntt.com; msnr.nakamura@ntt.com; yutaka.miyamoto@ntt.com).

Takushi Kazama and Takeshi Umeki are with the NTT Device Technology Laboratories, NTT Corporation, Atsugi 243-0198, Japan, and also with the NTT Network Innovation Laboratories, NTT Corporation, Yokosuka 239-0847, Japan (e-mail: takushi.kazama@ntt.com; takeshi.umeki@ntt.com).

Koji Enbutsu, Takahiro Kashiwazaki, and Masashi Abe are with the NTT Device Technology Laboratories, NTT Corporation, Atsugi 243-0198, Japan (e-mail: koji.enbutsu@ntt.com; takahiro.kashiwazaki@ntt.com; masashi.abe@ntt.com).

Tomoyuki Kato, Yu Tanaka, and Takeshi Hoshida are with the Fujitsu Limited, Kawasaki 212-8510, Japan (e-mail: kato.tom@fujitsu.com; yu\_tanaka@fujitsu.com; hoshida@fujitsu.com).

Color versions of one or more figures in this article are available at <https://doi.org/10.1109/JLT.2023.3323197>.

Digital Object Identifier 10.1109/JLT.2023.3323197

optical fiber networks, and the combined use of C- and L-bands (total:  $\sim$ 11 THz) supported by erbium-doped fiber amplifiers (EDFAs) has been well studied [1], [2], [3]. In recent years, the use of the S-band with a bandwidth of up to  $\sim$ 9 THz (1460–1530 nm) has also been actively investigated with a Raman amplifier [4], [5], [6], a thulium-doped fiber amplifier (TDFA) [7], and a semiconductor amplifier [8]. Using these triple S-, C-, and L-bands, a  $>$ 100-Tbps fiber throughput was demonstrated [5], [6], [7], [8]. As the next transmission band, the use of the E-band (1360–1460 nm), which has a shorter wavelength than the S-band, has been investigated with a bismuth-doped fiber amplifier (BDFa) and a Raman amplifier [9], [10]. However, full utilization of the E-band requires low-water-peak fibers as transmission lines, hindering fiber compatibility. The BDFa can also support the O-band (1260–1360 nm), which is an even shorter wavelength band than E-band [9], [11]. The O-band is located around the zero-dispersion wavelength of standard single-mode fiber (SMF) and has been considered for use in short-haul transmission systems. However, strong signal distortions caused by fiber nonlinearity in the O-band due to small chromatic dispersion will present a significant challenge when using it for long-haul dense-WDM transmission. The U-band, which has a longer wavelength than the L-band, is another promising transmission band. It spans over  $\sim$ 5.5 THz (1625–1675 nm) and has a low transmission loss regardless of fiber type. In addition, the U-band signal can obtain optical power from shorter-wavelength-band signals via inter-band stimulated Raman scattering (ISRS), and thus, the actual transmission loss of the U-band signal in multiband WDM transmission can be reduced well beyond that of the E- and O-bands [12], [13].

Because there is a lack of effective rare-earth-doped fiber amplifiers for the U-band, Raman amplification is the next candidate to achieve the U-band transmission. Recently, with forward- and backward-pumped distributed Raman amplification, a 285-km single-span transmission of an 18.4-Gbps BPSK signal up to 1651 nm was reported [14]. Moreover, a real-time 80-km transmission of a 200-Gbps dual-polarization (DP) QPSK signal allocated in the U-band up to 1650 nm was demonstrated with an ISRS gain from a co-propagated C+L-band WDM signal [13]. Meanwhile, there have been few demonstrations of

transmission using U-band WDM signal, except for a few reports in the early 2000s. One is a  $3 \times 40$ -km transmission of a 200-nm wideband WDM signal including a few U-band 10-Gbps non-return-to-zero (NRZ) channels up to 1661 nm with distributed Raman amplification [14]. A  $3 \times 75$ -km WDM transmission of 42.7-Gbps NRZ signals up to 1640 nm was also reported [16]. However, digital coherent dense-WDM transmission using the U-band with a spectral-efficient modulation format has not been demonstrated due to a lack of practical optical components supporting the U-band. Wavelength-selective switches (WSSs) partly supporting longer wavelengths beyond the L-band have become commercially available, but most optical components, especially for transceivers, are not practical for such a longer band in terms of laser linewidth [17] and photodiode sensitivity [18].

The optical parametric amplifier (OPA) has attracted attention for constructing wideband WDM systems because of its wide-gain bandwidth [19], [20], [21]. In addition, as with the Raman amplifier, the gain band can be shifted to various telecommunication bands by designing a phase matching for media and pump-frequency allocation [22], [23], [24]. There are two types of OPAs; one utilizes  $\chi^{(3)}$ -nonlinear media (e.g., highly nonlinear fiber) [20], [21], and the other utilizes  $\chi^{(2)}$ -nonlinear media. Over-10-THz high-gain bandwidth and wideband inline-amplified transmissions using OPAs with periodically poled LiNbO<sub>3</sub> (PPLN) waveguides as a  $\chi^{(2)}$ -nonlinear medium have been demonstrated [25], [26]. Another feature of the OPA is a wavelength conversion (spectral inversion) function utilizing the idler light generated simultaneously with the signal amplification. Inter-band wavelength conversion by OPAs enables conventional optical components to be used for additional bands as well, and its applications to multiband transceivers and optical cross-connects have been investigated [27], [28], [29], [30]. Therefore, U-band transmission is made possible with commercially available transceivers and other components by using inter-band wavelength conversion, and the demonstration of [13] was performed using wavelength conversion with highly nonlinear fibers.

This article describes our recent demonstration of L- and U-band inline-amplified transmission of a 60-channel 100-GHz-spaced WDM signal using a PPLN-based OPA [31]. PPLN-based OPAs, which have the advantage of low inter-channel cross-talk caused by unwanted nonlinear effects between WDM channels with the features of  $\chi^{(2)}$ -nonlinear media, can perform wideband simultaneous wavelength conversion while the signal is amplified with a high gain and high output power. The modulation format is 96-Gbaud probabilistically constellation-shaped (PCS) 36QAM with a net data rate of 640 Gbps/ch. A 6-THz dense-WDM signal within 1597.2–1649.9 nm (181.7–187.7 THz) is inline-amplified by PPLN-based OPAs and transmitted over  $5 \times 80$ -km G.654.E SMFs. The PPLN-based OPAs used as inline amplifiers have a 190.6-THz center frequency (1572.9 nm) for the gain band and can perform simultaneous wavelength conversion from L- and U-bands to S- and C-bands (or vice versa) while amplifying the WDM signal. Thus, we could perform gain equalization, WDM signal generation, and coherent reception without U-band optical components.

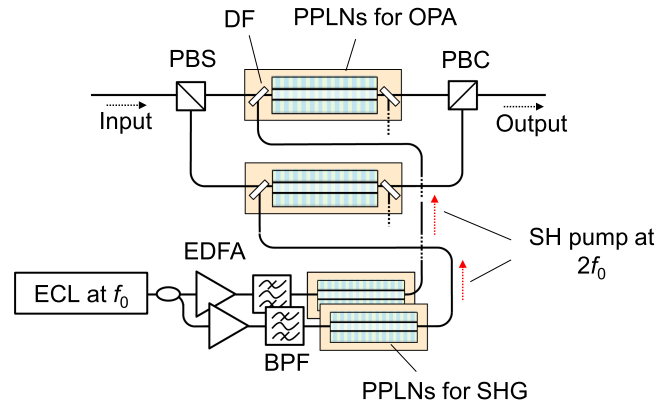


Fig. 1. Configuration of PPLN-based optical parametric amplifier.  $f_0$  is degenerate frequency of PPLN waveguides.

Moreover, by conducting wavelength conversion using OPAs with a 194.0-THz center frequency (1545.3 nm) on the receiver side, all signals are received in either the practical C-band or L-band. In addition, we report the signal amplification characteristics of the OPA and the transmission characteristics of the U-band signals in detail. In Section II, we describe the configuration of our PPLN-based OPA and its amplification characteristics. In Section III, the L- and U-band inline-amplified transmission experiment is described. Section III-A describes the experimental setup, which uses a recirculating loop, Section III-B describes an optical power design considering the gain saturation effect of the OPA and fiber nonlinearities, and Section III-C shows the results of the inline-amplified transmission. Finally, Section IV concludes this article.

## II. CHARACTERISTICS OF PPLN-BASED OPA

This section describes the amplification characteristics of the PPLN-based OPA used as an inline amplifier in this work. Fig. 1 shows the configuration of the PPLN-based OPA. Optical nonlinear effects are sensitive to polarization, so a polarization-diverse configuration is used in which two waveguides are sandwiched by a polarization-beam splitter (PBS) and a polarization-beam combiner (PBC) [19], [32]. The  $\chi^{(2)}$ -based optical parametric amplification process requires second harmonic (SH) pump light at twice the center frequency of the phase-matching band (gain band) of the waveguide. To obtain a watt-level SH pump, continuous wave (CW) light at the center frequency of the phase-matching band (degenerate frequency),  $f_0$ , with a  $<30$ -kHz linewidth is used as the pump light source, is amplified by the EDFA, and then, converted to SH pump at  $2f_0$  by second-harmonic generation (SHG) with a PPLN waveguide [33]. The PPLN waveguide and the dichroic filters for (de-) combining the signal and SH pump were integrated into a module for high-efficient optical parametric amplification [34].

The gain spectrum of the OPA depends on the phase-matching condition between signal, idler, and SH pump components [35]. In the PPLN waveguide used as a  $\chi^{(2)}$ -medium, the phase-mismatch amount depends on the effective refractive index of

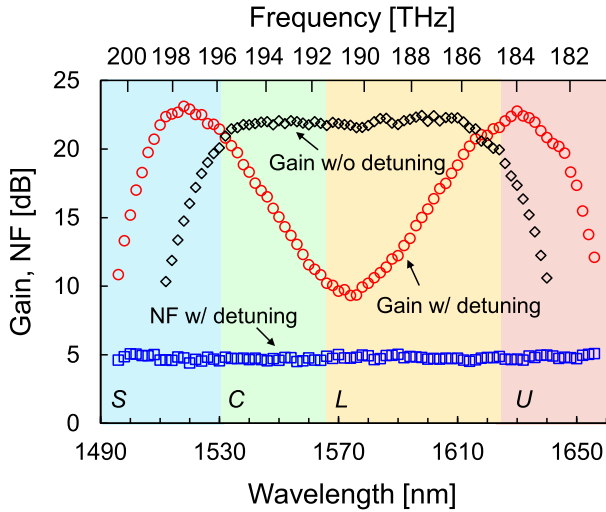


Fig. 2. Gain and NF spectra of our PPLN-based OPA with degenerate frequency of 190.6 THz (1572.89 nm) across S-, C-, L-, and U-bands.

the fundamental mode in the waveguide and the poling period [36]. The refractive index spectrum of the material depends on the temperature [37], and so does the phase-mismatch amount. Therefore, the gain spectrum of the PPLN waveguide depends on the waveguide temperature. To demonstrate inline U-band amplification using the PPLN-based OPA, we used PPLN waveguides fabricated for L-band applications with a degenerate frequency of 190.6 THz (1572.9 nm) [30]. By detuning the temperature of this PPLN waveguide from the optimal temperature for L-band use, the gain bandwidth was extended to the U-band.

Fig. 2 shows the gain and noise figure (NF) spectra of the polarization-diverse PPLN-based OPA for the inline optical amplifier. The power of the SH pump input to each PPLN was  $\sim 2.0$  W. We input CW light to the polarization-diverse OPA and measured its input and output spectra with an optical spectrum analyzer (OSA). The gain and NF were calculated by comparing these spectra [38]. The gain was calculated as the ratio of the peak powers of the CW-light input and output spectra measured at a resolution of 0.1 nm. The NF was calculated from the power density of the noise floor generated around the CW light in the output spectrum and the gain and was expressed as

$$F = \frac{1}{G} + \frac{P_{\text{ASE}}}{G \cdot h \cdot \nu \cdot \Delta\nu}, \quad (1)$$

where  $G$  is the gain,  $P_{\text{ASE}}$  is the noise floor obtained by the OSA,  $h$  is the Planck constant,  $\nu$  is the center frequency of the CW light, and  $\Delta\nu$  is the resolution of the OSA [38]. Without temperature detuning, the phase-matching condition was optimal around the degenerate frequency, and a flat-top gain spectrum covering the C- and L-bands was obtained. Meanwhile, with temperature detuning, the gain around the degenerate frequency significantly decreased, while the gain in the low and high-frequency bands increased. The maximum gain was obtained at  $\sim 184.15$  THz ( $\sim 1628$  nm), indicating that the phase-mismatch amount was near zero around this frequency. That is, the optimum phase-matching frequency was shifted by

$\sim 6.45$  THz with temperature detuning. As a result, a  $>15$ -dB-gain bandwidth over 6 THz within the L- and U-bands (181.7–187.7 THz, 1597.2–1649.9 nm) was achieved. In addition, an OPA can inter-convert between bands allocated at symmetrical frequencies with respect to  $f_0$ . Therefore, a PPLN-based OPA with an  $f_0$  of 190.6 THz could inter-convert between L- and U-band signals within 181.7–187.7 THz and S- and C-band signals within 193.5–199.5 THz (1502.7–1549.3 nm) (as shown in Fig. 3(c)) simultaneously with amplification. The conversion efficiency almost corresponds with the amplification gain in the high gain region [19]. The NF was  $\sim 5$  dB, which is comparable to a C-band EDFA. By utilizing the wavelength-band conversion function, we configured the recirculating transmission link to demonstrate the inline-amplified U-band WDM transmission without optical components supporting the U-band, which will be described in detail in the next section.

### III. 6-THz WDM TRANSMISSION OVER L- AND U-BANDS THROUGH $5 \times 80$ -KM G.654.E SMF

This section describes 6-THz WDM transmission over the L- and U-bands using optical parametric inline amplification and wavelength-band conversion. The optical transmission power design, which considers OPA nonlinearity and fiber nonlinearity, is also explained.

#### A. Experimental Setup

Fig. 3(a) shows the experimental setup for inline-amplified transmission of a 100-GHz-spaced 60-channel WDM signal using the L- and U-bands. We modulated only one channel at a time (channel under test (CUT)) and emulated the other WDM channels using amplified spontaneous emission (ASE). In this setup, the WDM signal transited over various bands by using wavelength conversion with multiple OPAs. The S- and C-band WDM signal was generated on the transmitter side and converted to the L- and U-band WDM signal using the OPA described in Section II in the recirculating loop. Fig. 3(b)–(d) show spectral transition diagrams for the transmitter side, the recirculating loop, and the receiver side. In addition, the frequency/wavelength/band allocation is also listed in detail in Table I. The bands in Table I are subdivided to clarify the spectral transitions at each point in the setup. In the following, we describe this setup in detail for the transmitter side, the recirculating loop, and the receiver side.

On the transmitter side, the CUT was generated as a 96-Gbaud Nyquist-pulse-shaped DP-PCS-36QAM optical signal with a roll-off factor of 0.03 using an I/Q modulator and polarization-division-multiplexing emulator (PDME) with a 15-m delay line between orthogonal polarization components. The entropy of the DP-PCS-36QAM signal was 8.87 bits per 4D symbol. The CUT was amplified by an EDFA or a TDFA depending on its frequency. Ch. 1–34 at 193.5–196.9 THz ( $C_{\text{Tx}}$ ) were amplified by a C-band EDFA, and ch. 35–60 at 196.9–199.5 THz ( $S_{\text{Tx}}$ ) were amplified by a TDFA. The channels were numbered in order of lower frequency (longer wavelength) in the S- and C-bands. A 100-GHz-spaced 60-channel WDM signal was emulated by ASE from EDFAs and WSS. Fig. 3(b) illustrates the spectral

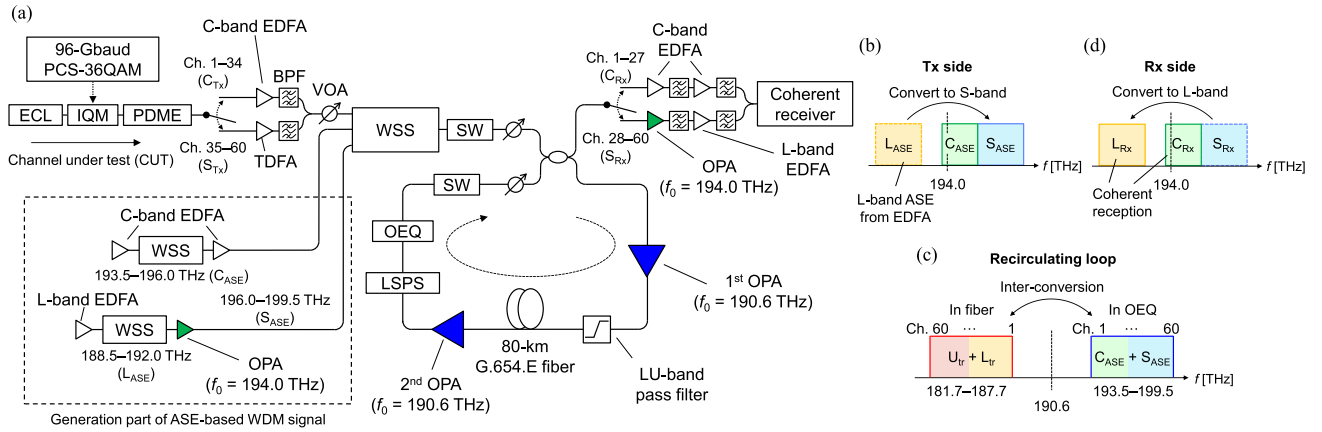


Fig. 3. Experimental setup for 6-THz inline-amplified WDM transmission using L- and U-bands. (a) Detailed schematic illustration. ECL: External cavity laser, IQM: I/Q modulator, PDME: Polarization-division-multiplexing emulator, BPF: Band-pass filter, VOA: Variable optical attenuator, WSS: Wavelength-selective switch, SW: Optical switch, LSPS: Loop-synchronous polarization scrambler, and OEQ: Optical equalizer. (b)–(d) Spectral transition on transmitter (Tx) side, recirculating loop, and receiver (Rx) side.

TABLE I  
FREQUENCY/WAVELENGTH/BAND ALLOCATION OF CUT AND ASE-BASED WDM SIGNAL

	$f$ [THz]	$\lambda$ [nm]	Band
Tx side			
Ch. 1–34	193.5–196.9	1522.6–1549.3	$C_{Tx}$
Ch. 35–60	196.9–199.5	1502.7–1522.6	$S_{Tx}$
C-band ASE	193.5–196.0	1529.6–1549.3	$C_{ASE}$
L-band ASE	188.5–192.0	1561.4–1590.4	$L_{ASE}$
S-band ASE	196.0–199.5	1502.7–1529.6	$S_{ASE}$
Recirculating loop			
In G.654.E SMF	181.7–187.7	1597.2–1649.9	$L_{tr} + U_{tr}$ ( $C_{ASE} + S_{ASE}$ )
In OEQ	193.5–199.5	1502.7–1549.3	$C_{ASE} + S_{ASE}$
Rx side			
Ch. 1–27	193.5–196.2	1528.0–1549.3	$C_{Rx}$
Ch. 28–60	196.2–199.5	1502.7–1528.0	$S_{Rx}$
Ch. 28–60 *	188.5–191.8	1563.0–1590.4	$L_{Rx}$ ( $S_{Rx}$ )

\* denotes spectral inversion.

transition on the transmitter side in our setup. To generate an L- and U-band WDM signal with spectral inversion using the OPA with an  $f_0$  of 190.6 THz in the recirculating loop (as shown in Fig. 3(c)), we generated a broad ASE over 193.5–199.5 THz in the S- and C-bands on the transmitter side. The C-band WDM signal was generated by shaping the ASE output of the C-band EDFA to 193.5–196.0 THz ( $C_{ASE}$ ) with the WSS. To obtain a high-power S-band ASE, the ASE from an L-band EDFA was amplified and converted to the S-band using a PPLN-based OPA whose  $f_0$  was 194.0 THz (1545.3 nm) [25]. This OPA converted the L-band ASE shaped at 188.5–192.0 THz ( $L_{ASE}$ ) with the WSS to the S-band ASE within 196.0–199.5 THz ( $S_{ASE}$ ) as shown in Fig. 3(b). The C-band ASE, S-band ASE, and CUT were combined by using a WSS and input to a recirculating loop. As it will be discussed in the next subsection, gain saturation occurs in the OPA as the pump depletes in the high-output power

region. To efficiently input the optical power to the transmission line with the output power limited by gain saturation, it is effective to pre-equalize the input light of the OPA with the inverse profile of the gain spectrum; this is possible because the gain spectrum of the OPA is independent of the spectrum and power of the input light (in the unsaturated region). Therefore, in the WSS, the WDM signal was pre-equalized with an inverse profile of the gain spectrum of the 1st OPA in the recirculating loop.

The recirculating loop consisted of an 80-km G.654.E SMF, two PPLN-based OPAs, a loop-synchronous polarization scrambler (LSPS), an optical equalizer (OEQ), an optical switch (SW), and a variable optical attenuator (VOA). In the loop, the WDM signal was transmitted while repeating wavelength-band conversion simultaneously with inline amplification by the OPA with an  $f_0$  of 190.6 THz as shown in Fig. 3(c). First, the WDM signal at 193.5–199.5 THz was amplified and converted to 181.7–187.7 THz ( $L_{tr} + U_{tr}$ ) in the L- and U-bands by using the 1st OPA with the  $f_0$  of 190.6 THz (1572.9 nm). Although the output of the 1st OPA had a signal component (193.5–199.5 THz) and idler component (181.7–187.7 THz), the idler component was extracted by using an L- and U-band-pass filter. Then, the L- and U-band WDM signal was propagated with an 80-km transmission line consisting of 30-km and 50-km G.654.E fibers wound on bobbins with a 20-cm diameter. The ordering of channels after the wavelength-band conversion to the L- and U-bands were inverted with respect to the original ordering in S- and C-bands because the WDM signal was spectrally inverted as shown in Fig. 3(c). Fig. 4 shows the transmission loss of the 80-km G.654.E fiber. The loss was  $\sim 14.5$  dB up to 188.5 THz in the low-loss band following the C-band and increased with longer wavelengths thereafter. At 181.7 THz ( $\sim 1650$  nm) as the lowest frequency (longest wavelength) of the WDM signal, it was  $\sim 16.8$  dB. This large transmission loss of the U-band may be greatly reduced by ISRS in multiband transmission where C-band signals are co-transmitted [13]. The transmitted WDM signal was amplified and re-converted to the S- and C-bands by

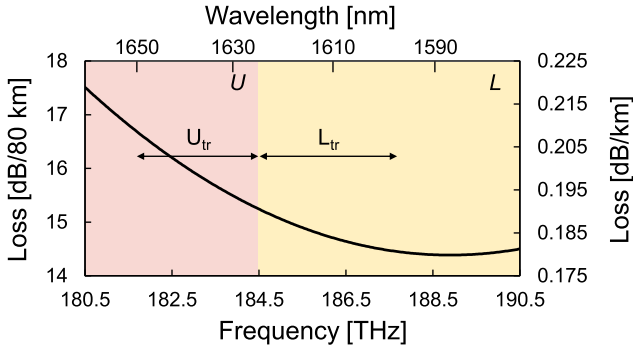


Fig. 4. Loss spectrum of 80-km G.654.E SMF.

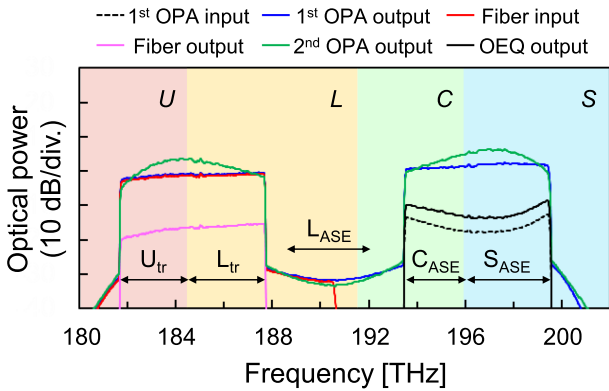


Fig. 5. Optical spectra at each point.

the 2nd OPA. Then, gain equalization was performed by an OEQ that supports C- and S-bands. The OEQ shaped the spectrum of the WDM signal to the same spectrum as the input to the recirculating loop. The gain spectra of the 1st and 2nd OPAs were almost the same, and the dual-gain-block structure [26] with those two OPAs compensated for the link loss. Fig. 5 shows the optical spectra at each point in the recirculating loop. As we can see, the 1st OPA input spectrum in the S- and C-bands was curved with the inverse profile of the gain spectrum of the OPA due to the pre-equalization on the transmitter side, and thus, the fiber input spectrum in the L- and U-bands was flattened. Moreover, we confirmed that the PPLN-based OPAs provide sufficient gain for inline amplification of the WDM signal. Excessive link gain was suppressed by the VOA.

On the receiver side, the CUT in the S- or C-bands was pre-amplified by different amplification stages depending on its frequency. Ch. 1–27 at 193.5–196.2 THz ( $C_{Rx}$ ) were amplified with 2-stage C-band EDFAs. Ch. 28–60 at 196.2–199.5 THz ( $S_{Rx}$ ) were converted to 188.5–191.8 THz ( $L_{Rx}$ ) with an OPA whose  $f_0$  was 194.0 THz, and then, amplified with the L-band EDFA (as shown in Fig. 3(d)). This was the reverse process of that used to generate the S-band ASE on the transmitter side. The amplified CUT was extracted by band-pass filters (BPFs) and received by a coherent receiver. Thus, all of the CUTs were received in the conventional transmission bands (C- or L-bands) thanks to wavelength conversion. The received signal was demodulated with offline digital signal processing

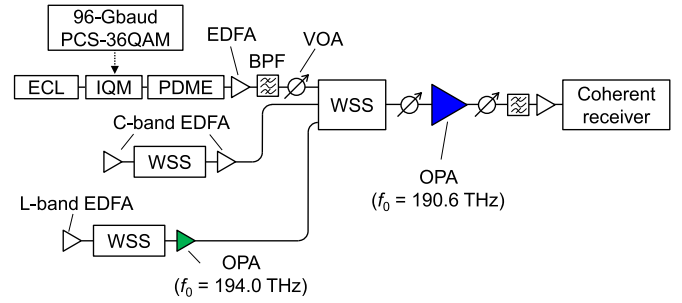


Fig. 6. Experimental setup for evaluating effect of gain saturation.

on the basis of an  $8 \times 2$  adaptive equalizer (AEQ) [39], and a normalized generalized mutual information (NGMI) was calculated. The AEQ was updated by a decision-directed least mean square (LMS) algorithm and pilot-aided LMS algorithm using pilot symbols periodically inserted into the signal. We assumed concatenated code for a low-density parity-check code and a BCH code with a code rate of 0.826. The net data rate of the signal was 640 Gbps/ch. with a NGMI threshold of 0.857 also assuming 1.64% pilot insertion [25].

### B. Optical Power Design

One of the challenges of the OPA is the gain saturation due to pump depletion, which causes nonlinear signal distortion [40]. Therefore, we evaluated the input power characteristics of our PPLN-based OPA before transmission experiments. Fig. 6 shows the experimental setup for evaluating the effect of the gain saturation on the signal quality. The transmitter side was the same as the setup shown in Fig. 3(a), and the WDM signal was pre-equalized as shown in Fig. 5. The CUT was ch. 20 at a center frequency of 195.45 THz in the S- and C-band WDM signal. The S- and C-bands WDM signal was input to the PPLN-based OPA with varying power using the VOA. After the amplification, the CUT at 195.45 THz was extracted by the BPF, amplified by the EDFA, and received by the coherent receiver. To evaluate only the effect of the gain saturation, the input power to the EDFA on the receiver side was set to  $-25$  dBm regardless of the OPA input power. Fig. 7(a) shows the gain dependence on the input power of the S- and C-band WDM signal. The gain did not depend on the input power in the low-power region, but it decreased nonlinearly as the input power increased in the high-power region due to pump depletion. Due to the fast time response of the OPA, this gain nonlinearity occurs symbol-by-symbol. Therefore, higher power symbols (the outer symbols on a constellation diagram) are subject to greater gain reduction, resulting in nonlinear amplitude distortion in the signal [40]. Fig. 7(b) shows the dependence of the signal-to-noise ratio (SNR) and NGMI on the input power to the OPA. At  $>4$  dBm, a slight degradation in signal quality was observed. Therefore, the dependence of signal quality on fiber-launched power in multi-span transmission using inline OPAs is affected not only by fiber nonlinearities but also by the nonlinearity of the OPAs.

Next, we evaluated the fiber-launched power dependence with the setup shown in Fig. 3(a). We determined the fiber-launched

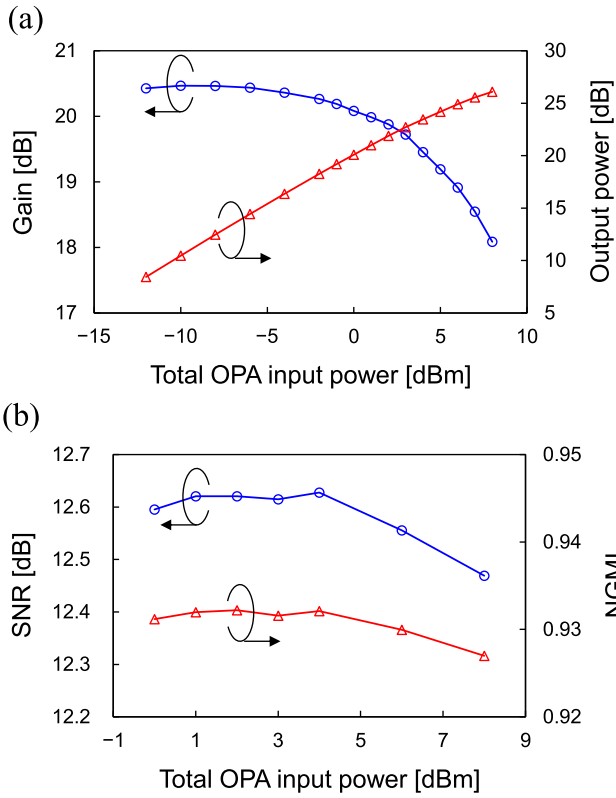


Fig. 7. OPA performance for input power. (a) Gain saturation. (b) Signal quality at ch. 20 (center frequency of 195.45 THz).

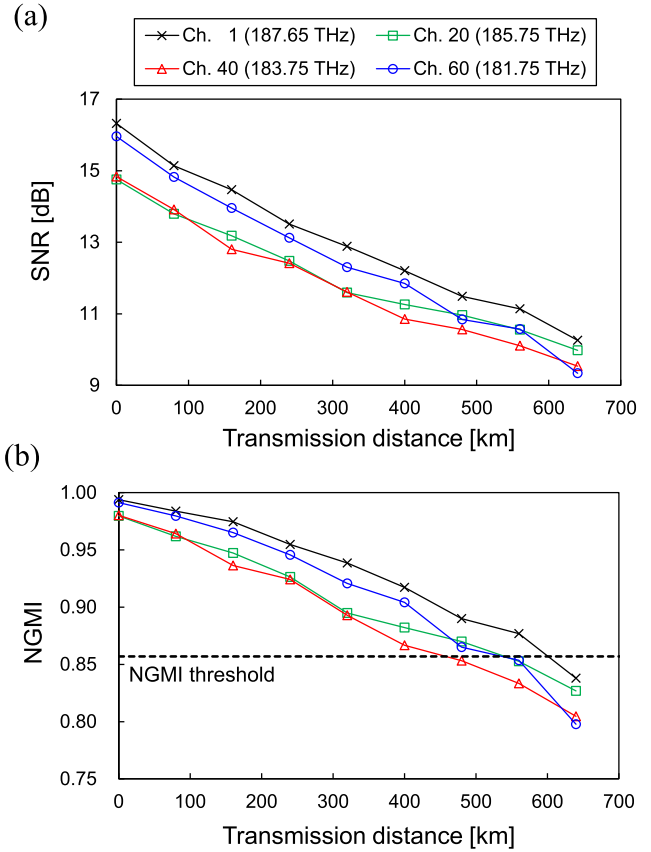


Fig. 9. (a) SNR and (b) NGMI as function of transmission distance.

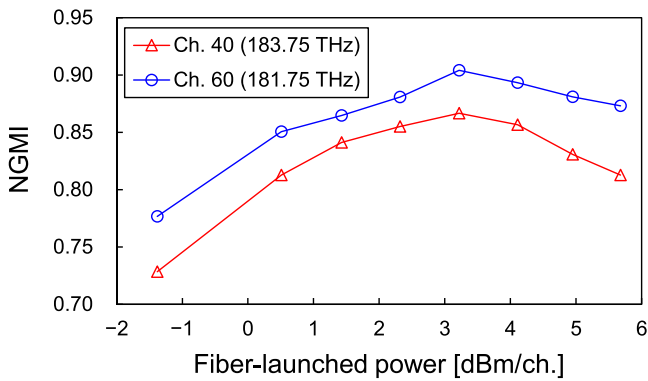


Fig. 8. Dependence of NGMI of DP-PCS-36QAM signal on fiber-launched power after  $5 \times 80$ -km inline-amplified transmission at ch. 40 and 60 (center frequencies of 183.75 and 181.75 THz).

power that gave the best NGMI performance for the spectral shapes of the WDM signal shown in Fig. 5. The CUTs were set to ch. 40 and 60 at center frequencies of 183.75 and 181.75 THz, respectively. The fiber-launched power was controlled by the VOA at the input of the recirculating loop. Therefore, the dependence included not only the fiber nonlinearity but also the OPA nonlinearity. Fig. 8 shows the measurement results after a  $5 \times 80$ -km transmission. The difference in NGMIs between ch. 40 and 60 was due to the pre-equalization. In this setup, the 1st OPA functioned as a booster amplifier in the 1st lap

and as a post-amplifier in the subsequent laps. Therefore, it was necessary to attenuate the input power to the 1st OPA to the recirculating loop input power at each lap. Thus, the shape of the pre-equalization was the dominant factor for determining the optical SNR (OSNR) in each channel. Ch. 60, which had less attenuation in pre-equalization, had a better signal quality than ch. 40. Meanwhile, the optimal fiber-launched power was 3.2 dBm/ch. for both channels. The total WDM power was 21 dBm, and the input power to the 1st OPA was  $\sim 1$  dBm, at which the signal distortion caused by the OPA was negligible according to the pre-measurement shown in Fig. 7. Therefore, the measured NGMIs simply depended on the OSNR and fiber nonlinearity.

### C. Transmission Results

Fig. 9 shows the transmission distance dependence of the signal quality up to 640 km ( $8 \times 80$  km). With a back-to-back configuration (0 km), ch. 1 (187.65 THz) and 60 (181.75 THz), at which the attenuation in the pre-equalization was small were better than ch. 20 (185.75 THz) and 40 (183.75 THz). Ch. 20 and 40 had the same quality due to almost the same attenuation amount in the pre-equalization. As the transmission distance increased, the quality of ch. 60 degraded more rapidly than ch. 1. The same trend was observed between ch. 20 and 40. This is due to the larger transmission loss in the U-band. The quality of

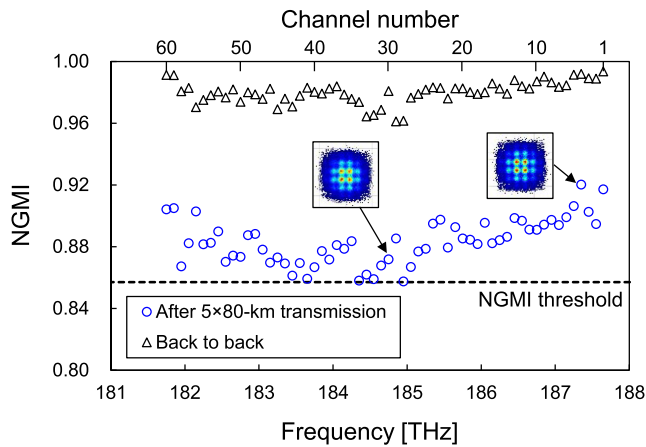


Fig. 10. NGMI of all 60 channels before and after 400-km ( $5 \times 80$ -km) inline-amplified transmission.

all measured channels was better than the NGMI threshold up to 400 km ( $5 \times 80$  km).

Fig. 10 shows the NGMI of all channels after a  $5 \times 80$ -km transmission. As we can see, the back-to-back characteristic depended on the profile of the pre-equalization. The NGMI spectrum after the transmission was also characterized along the attenuation spectrum of the pre-equalization. Since the number of transmission spans was small, the attenuation in pre-equalization was the dominant factor for determining the OSNR rather than the loss of the transmission fiber. Meanwhile, all 60 channels were better than the NGMI threshold of 0.857, and 38.4-Tbps ( $60 \text{ ch.} \times 640 \text{ Gbps}$ ) transmission was successfully demonstrated.

In this experiment, we equalized the WDM spectrum input to the OPA with the inverse profile of its gain spectrum to fully utilize the unsaturated output power of the OPA. However, to optimize the transmission quality, it may be necessary to optimize the shape of the pre-equalization as well as the total launched power, taking into account the balance between OSNR degradation due to the pre-equalization and the OPA nonlinearity.

#### IV. CONCLUSION

We demonstrated 400-km ( $5 \times 80$  km) WDM transmission over 6 THz within L- and U-bands with 60-channel 96-Gbaud DP-PCS-36QAM signals using PPLN-based optical parametric amplification and wavelength-band conversion. Our PPLN-based OPAs provided an over-15-dB gain within 181.7–187.7 THz (1597.2–1649.9 nm). A dual-gain-block structure using two OPAs enabled inline-amplified transmission over an 80-km-span G.654.E SMF link.

We measured the gain saturation characteristic of our OPA and evaluated the dependence of the amplified signal quality on the input power to our OPA. We also evaluated the fiber-launched power dependence of the transmitted signal quality, including the nonlinearity of the OPA. Under the experimental condition, there was little effect of OPA nonlinearity, and the best fiber-launched power was determined to be 3.2 dBm/ch.

(total power of 21 dBm) due to the effect of fiber nonlinearity. We also evaluated signal quality as a function of transmission distance, and it was found that U-band channels were degraded more rapidly than L-band channels as the number of spans increased due to the transmission loss spectrum. This excessive degradation in the U-band channels may be suppressed by ISRS in wider bandwidth transmission.

As a result of the inline-amplified transmission, a total net data rate of 38.4 Tbps ( $60 \text{ ch.} \times 640 \text{ Gbps}$ ) was achieved after 400-km transmission. Utilizing the wavelength-band conversion function of the OPA, we achieved U-band transmission without optical components supporting the U-band such as transceivers and a WSS. These results indicate the potential for multiband optical networks including the U-band with an OPA.

#### REFERENCES

- [1] H. Masuda et al., “20.4 Tb/s ( $204 \times 111$  Gb/s) Transmission over 240 km using bandwidth-maximized hybrid Raman/EDFAs,” in *Proc. Opt. Fiber Commun. Conf.*, 2007, Paper PDP20.
- [2] A. Ghazisaeidi et al., “Advanced C+L-band transoceanic transmission systems based on probabilistically shaped PDM64QAM,” *J. Lightw. Technol.*, vol. 35, no. 7, pp. 1291–1299, Apr. 2017.
- [3] M. Ionescu et al., “74.38 Tb/s transmission over 6300 km single mode fiber with hybrid EDFA/Raman amplifiers,” in *Proc. Opt. Fiber Commun. Conf.*, 2019, pp. 1–3.
- [4] M. A. Iqbal, L. Krzczanowicz, I. Phillips, P. Harper, and W. Forysiak, “150 nm SCL-band transmission through 70 km SMF using ultra-wideband dual-stage discrete Raman amplifier,” in *Proc. Opt. Fiber Commun. Conf.*, 2020, Paper W3E.4.
- [5] B. J. Puttnam, R. S. Luís, G. Rademacher, M. Mendez-Astudillio, Y. Awaji, and H. Furukawa, “S-, C- and L-band transmission over a 157 nm bandwidth using doped fiber and distributed Raman amplification,” *Opt. Exp.*, vol. 30, no. 6, pp. 10011–10018, Mar. 2022.
- [6] X. Zhao et al., “200.5 Tb/s transmission with S+C+L amplification covering 150 nm bandwidth over  $2 \times 100$  km PSCF spans,” in *Proc. IEEE Eur. Conf. Exhib. Opt. Commun.*, 2022, pp. 1–4.
- [7] F. Hamaoka, M. Nakamura, M. Takahashi, T. Kobayashi, Y. Miyamoto, and Y. Kisaka, “173.7Tb/s triple-band WDM transmission using 124-channel 144-Gbaud signals with SE of 9.33 b/s/Hz,” in *Proc. IEEE Opt. Fiber Commun. Conf. Exhib.*, 2023, pp. 1–3.
- [8] J. Renaudier et al., “First 100-nm continuous-band WDM transmission system with 115 Tb/s transport over 100km using novel ultra-wideband semiconductor optical amplifiers,” in *Proc. IEEE Eur. Conf. Opt. Commun.*, 2017, pp. 1–3.
- [9] Y. Wang, N. K. Thipparapu, D. J. Richardson, and J. K. Sahu, “Ultra-broadband bismuth-doped fiber amplifier covering a 115nm bandwidth in the O and E bands,” *J. Lightw. Technol.*, vol. 39, no. 3, pp. 795–800, Feb. 2021.
- [10] P. Hazarika, A. Donodin, M. Tan, I. Phillips, P. Harper, and W. Forysiak, “30-Gbaud PM-16-QAM transmission over E-, S-, C- and L-band with hybrid Raman amplifier,” in *Proc. IEEE Opt. Fiber Commun. Conf. Exhib.*, 2023, pp. 1–3.
- [11] D. J. Elson et al., “9.6-THz single fibre amplifier O-band coherent DWDM transmission,” in *Proc. IEEE Opt. Fiber Commun. Conf. Exhib.*, 2023, pp. 1–3.
- [12] T. Hoshida et al., “Ultrawideband systems and networks: Beyond C + L-band,” *Proc. IEEE*, vol. 110, no. 11, pp. 1725–1741, Nov. 2022.
- [13] T. Kato, H. Irie, H. Muranaka, Y. Tanaka, Y. Akiyama, and T. Hoshida, “U-band transmission of real time 200 Gb/s signal Co-propagating with C+L-band WDM signal,” in *Proc. IEEE Opt. Fiber Commun. Conf.*, 2023, pp. 1–3.
- [14] N. Taengnoi, K. R. H. Bottrill, Y. Hong, L. Hanzo, and P. Petropoulos, “Broadband incoherently pumped Raman amplification for ultra-long span U-band transmission systems,” in *Proc. IEEE Eur. Conf. Opt. Commun.*, 2021, pp. 1–4.
- [15] T. Tanaka, K. Torii, M. Yuki, H. Nakamoto, T. Naito, and I. Yokota, “200-nm bandwidth WDM transmission around 1.55  $\mu\text{m}$  using distributed Raman amplifier,” in *Proc. IEEE Eur. Conf. Opt. Commun.*, 2002, pp. 1–2.

- [16] T. Matsuda, A. Matsuura, T. Kotanigawa, and T. Kataoka, "54×42.7 Gb/s L and U-band WDM signal transmission experiments using homogeneous dispersion line with inline hybrid optical amplifiers," in *Proc. Eur. Conf. Opt. Commun.*, 2003, Paper Tu1.6.4.
- [17] C. H. Henry, "Theory of the linewidth of semiconductor lasers," *J. Quantum Electron.*, vol. 18, no. 2, pp. 259–264, Feb. 1982.
- [18] H. Yamagishi, Y. Suzuki, and A. Hiraide, "Precise measurement of photodiode spectral responses using the calorimetric method," *IEEE Trans. Instrum. Meas.*, vol. 38, no. 2, pp. 578–580, Apr. 1989.
- [19] S. Shimizu et al., "PPLN-based optical parametric amplification for wideband WDM transmission," *J. Lightw. Technol.*, vol. 40, no. 11, pp. 3374–3384, Jun. 2022.
- [20] R. Malik, A. Kumpera, M. Karlsson, and P. A. Andrekson, "Demonstration of ultra wideband phase-sensitive fiber optical parametric amplifier," *Photon. Technol. Lett.*, vol. 28, no. 2, pp. 175–177, Dec. 2015.
- [21] V. Gordienko, F. M. Ferreira, C. B. Gaur, and N. J. Doran, "Looped polarization-insensitive fiber optical parametric amplifiers for broadband high gain applications," *J. Lightw. Technol.*, vol. 39, no. 19, pp. 6045–6053, Oct. 2021.
- [22] S. Shimizu et al., "Inter-band non-degenerate phase-sensitive amplification scheme for low-noise full C-band transmission," *Inst. Electron. Inf. Commun. Engineers Commun. Exp.*, vol. 11, no. 1, pp. 64–69, Jan. 2022.
- [23] C. B. Gaur, V. Gordienko, P. Hazarika, and N. J. Doran, "Polarization insensitive fiber optic parametric amplifier with a gain bandwidth of 22 nm in S-band," in *Proc. IEEE Opt. Fiber Commun. Conf.*, 2022, pp. 1–3.
- [24] C. B. Gaur, V. Gordienko, A. A. I. Ali, P. Hazarika, A. Ellis, and N. J. Doran, "Polarization-insensitive fibre optic parametric amplifier with gain bandwidth of 35 nm in L-band," in *Proc. IEEE Eur. Conf. Opt. Commun.*, 2021, 1–4.
- [25] T. Kobayashi et al., "Wide-band inline-amplified WDM transmission using PPLN-based optical parametric amplifier," *J. Lightw. Technol.*, vol. 39, no. 3, pp. 787–794, Feb. 2021.
- [26] T. Kobayashi et al., "103ch. 132Gbaud PS-QAM signal inline-amplified transmission with 14.1 THz bandwidth lumped PPLN-based OPAs over 400 km G.652.D SMF," in *Proc. Opt. Fiber Commun. Conf.*, 2023, Paper Th4B.6.
- [27] C. Guo, A. Shamschooli, Y. Akasaka, P. Palacharla, and M. Vasilyev, "Investigation of hybrid S-band amplifier performance with 8-channel × 10 Gbaud 16-QAM signals," in *Proc. IEEE Eur. Conf. Opt. Commun.*, 2021, pp. 1–3.
- [28] T. Kato et al., "Real-time transmission of 240×200Gb/s signal in S+C+L triple-band WDM without S or L-band transceivers," in *Proc. IEEE 45th Eur. Conf. Opt. Commun.*, 2019, pp. 1–4.
- [29] T. Kato et al., "S+C+L-band WDM transmission using 400Gb/s real-time transceivers extended by PPLN-based wavelength converter," in *Proc. IEEE Eur. Conf. Opt. Commun.*, 2022, pp. 1–4.
- [30] H. Minami et al., "Experimental demonstration of cascaded PPLN-based inter-band wavelength converters for band-switchable multi-band optical cross-connect," in *Proc. IEEE Opt. Fiber Commun. Conf.*, 2023, pp. 1–3.
- [31] S. Shimizu et al., "38.4 Tbps inline-amplified transmission using PPLN-based optical parametric amplifier over 6 THz within L and U-bands," in *Proc. Opt. Fiber Commun. Conf.*, 2023, Paper Th3F.3.
- [32] F. Bessin, V. Gordienko, F. M. Ferreira, and N. Doran, "First Experimental Mach-Zehnder FOPA for polarization and wavelength-division-multiplexed signals," in *Proc. IEEE Eur. Conf. Opt. Commun.*, 2021, pp. 1–3.
- [33] T. Kazama, T. Umeki, M. Abe, K. Enbutsu, Y. Miyamoto, and H. Takenouchi, "Low-parametric-crosstalk phase-sensitive amplifier for guard-band-less DWDM signal using PPLN waveguides," *J. Lightw. Technol.*, vol. 35, no. 4, pp. 755–761, Feb. 2017.
- [34] T. Kazama et al., "Over-30-dB gain and 1-dB noise figure phase-sensitive amplification using pump-combiner-integrated fiber I/O PPLN module," *Opt. Exp.*, vol. 29, no. 18, pp. 28824–28834, Aug. 2021.
- [35] R. W. Boyd, *Nonlinear Optics*, 4th ed. Amsterdam, The Netherlands: Elsevier, 2020.
- [36] T. Yanagawa et al., "Simultaneous observation of CO isotopomer absorption by broadband difference-frequency generation using a direct-bonded quasi-phase-matched LiNbO<sub>3</sub> waveguide," *Opt. Lett.*, vol. 31, no. 7, pp. 960–962, Apr. 2006.
- [37] D. H. Jundt, "Temperature-dependent Sellmeier equation for the index of refraction,  $n_e$ , in congruent lithium niobate," *Opt. Lett.*, vol. 22, no. 20, pp. 1553–1555, Oct. 1997.
- [38] M. Asobe, T. Umeki, and O. Tadanaga, "Phase sensitive amplification with noise figure below the 3 dB quantum limit using CW pumped PPLN waveguide," *Opt. Exp.*, vol. 20, no. 12, pp. 13164–13172, May 2012.
- [39] T. Kobayashi et al., "35Tb/s C-band transmission over 800 km employing 1Tb/s PS-64QAM signals enhanced by complex 8×2 MIMO equalizer," in *Proc. Opt. Fiber Commun. Conf.*, 2019, Paper Th4B.2.
- [40] S. Shimizu et al., "Effect of gain saturation on wideband WDM signal in PPLN-based optical parametric amplifier," *J. Lightw. Technol.*, vol. 41, no. 15, pp. 4922–4932, Aug. 2023.

**Shimpei Shimizu** (Member, IEEE) received the B.E. degree in engineering and the M.E. degree in information science and technology in the field of electronics for informatics from Hokkaido University, Sapporo, Japan, in 2016 and 2018, respectively. In 2018, he joined the NTT Network Innovation Laboratories, Yokosuka, Japan. His research is focuses on high-capacity optical transmission systems. He is a Member of the Institute of Electronics, Information and Communication Engineers, Tokyo, Japan, and IEEE Photonics Society.

**Takayuki Kobayashi** (Member, IEEE) received the B.E., M.E., and Dr. Eng. degrees from Waseda University, Tokyo, Japan, in 2004, 2006, and 2019, respectively. In April 2006, he joined the NTT Network Innovation Laboratories, Yokosuka, Japan, where he was engaged in the research on high-speed and high-capacity digital coherent transmission systems. In April 2014, he moved to the NTT Access Network Service Systems Laboratories, Yokosuka, and was engaged in 5G mobile optical network systems. He moved back to the NTT Network Innovation Laboratories and since July 2016, has been working on high-capacity optical transmission systems. His research interests include long-haul optical transmission systems employing spectrally efficient modulation formats enhanced by digital and optical signal processing. He is a Member of the Institute of Electronics, Information and Communication Engineers, Tokyo, Japan. From 2016 to 2018, he was a Technical Program Committee Member of the Electrical Subsystems' Category for the Optical Fiber Communication Conference. Since 2018, he has been a TPC Member of the Point-to-Point Optical Transmission Category for the European Conference on Optical Communication.

**Akira Kawai** (Member, IEEE) received the B.S. and M.S. degrees from the University of Tokyo, Tokyo, Japan, in 2018 and 2020, respectively. In 2020, he joined the NTT Network Innovation Laboratories, Yokosuka, Japan. His research is focuses on high-capacity optical transmission systems. He is a Member of the Institute of Electronics, Information and Communication Engineers, Tokyo.

**Takushi Kazama** received the B.S. and M.S. degrees in electrical engineering from The University of Tokyo, Tokyo, Japan, in 2009 and 2011, respectively. In 2011, he joined the NTT Device Technology Laboratories, Atsugi, Japan, where he is engaged in research on nonlinear optical devices based on periodically poled LiNbO<sub>3</sub> waveguides. He is a Member of the Institute of Electronics, Information, and Communication Engineers, Tokyo, and Japan Society of Applied Physics.

**Masanori Nakamura** (Member, IEEE) received the B.S. and M.S. degrees in applied physics from Waseda University, Tokyo, Japan, in 2011 and 2013, respectively, and the Ph.D. degree in electrical, electronic, and infocommunications engineering from Osaka University, Osaka, Japan, in 2021. In 2013, he joined NTT Network Innovation Laboratories, Yokosuka, Japan, where he engaged in research on high-capacity optical transport networks. He is a Member of the Institute of Electronics, Information and Communication Engineers, Tokyo. He was the recipient of the 2016 IEICE Communications Society Optical Communication Systems Young Researchers Award.

**Koji Enbutsu** received the B.E. and M.E. degrees in electronics engineering from Hokkaido University, Sapporo, Japan, in 1994 and 1996, respectively. In 1996, he joined the NTT Opto-Electronics Laboratories, Japan, where he engaged in research on organic optical waveguides for optical communications and electro-optic crystals and their devices. In 2007, he moved to the NTT Access Services Network System Laboratories, where he engaged in research on optical fiber testing and monitoring. He is a Member of the Institute of Electronics, Information, and Communication Engineers, and Japan Society of Applied Physics.

**Takahiro Kashiwazaki** received the B.E. and M.E. degrees in materials science from Keio University, Tokyo, Japan, in 2013 and 2015, respectively. He joined the NTT Device Technology Laboratories, Atsugi, Japan, in 2015. He is conducting research on periodically poled lithium niobate waveguide devices. He is a Member of the Institute of Electronics, Information, and Communication Engineers, Tokyo, and Japan Society of Applied Physics.

**Masashi Abe** received the B.S. and M.S. degrees in physics and the Ph.D. degree in the area of quantum electronics from Keio University, Tokyo, Japan, in 2006, 2008, and 2015, respectively. In 2015, he joined the NTT Device Technology Laboratories, Atsugi, Japan, where he was involved in research on the application of periodically poled lithium niobate waveguide devices. In 2017, he joined Chuo University, Tokyo, where he was engaged in research on the atomic physics. In 2022, he rejoined the NTT Device Technology Laboratories. He is a Member of the Physical Society of Japan and Spectroscopical Society of Japan.

**Takeshi Umeki** (Member, IEEE) received the B.S. degree in physics from Gakushuin University, Tokyo, Japan, in 2002, and the M.S. degree in physics and the Ph.D. degree in nonlinear optics from The University of Tokyo, Tokyo, in 2004 and 2014, respectively. He joined the NTT Photonics Laboratories, Atsugi, Japan, in 2004, since then he has been involved in research on nonlinear optical devices based on periodically poled LiNbO<sub>3</sub> waveguides. He is a Member of the Japan Society of Applied Physics, Institute of Electronics, Information, and Communication Engineers, and IEEE/Photonics Society.

**Yutaka Miyamoto** (Member, IEEE) received the B.E. and M.E. degrees in electrical engineering from Waseda University, Tokyo, Japan, in 1986 and 1988, respectively, and the Dr. Eng. degree in electrical engineering from Tokyo University, Tokyo, in 2016. In 1998, he joined the NTT Transmission Systems Laboratories, Yokosuka, Japan, where he was engaged in the research and development of high-speed optical communications systems including the 10-Gbit/s first terrestrial optical transmission system (FA-10G) using erbium-doped fiber amplifiers inline repeaters. From 1995 to 1997, he was with the NTT Electronics Technology Corporation, Yokohama, Japan, where he was engaged in the planning and product development of high-speed optical module at the data rate of 10 Gb/s and beyond. Since 1997, he has been with the NTT Network Innovation Laboratories, Yokosuka, where he has contributed to the research and development of optical transport technologies based on 40/100/400-Gbit/s channel and beyond. He is currently an NTT Fellow and the Director of the Innovative Photonic Network Research Center, NTT Network Innovation Laboratories, where he has been investigating and promoting the future scalable optical transport network with the Pbit/s-class capacity based on innovative transport technologies such as digital signal processing, space division multiplexing, and cutting-edge integrated devices for photonic preprocessing. He is a Fellow of the Institute of Electronics, Information, and Communication Engineers.

**Tomoyuki Kato** (Member, IEEE) received the B.E., M.E., and Dr. Eng. degrees in electronic engineering from Yokohama National University, Yokohama, Japan, in 2001, 2003, and 2006, respectively. From 2006 to 2009, he was a Research Associate with the Precision and Intelligence Laboratories, Tokyo Institute of Technology, Tokyo, Japan. Since he joined Fujitsu Laboratories Ltd., Kawasaki, Japan, in 2009, he has been engaged in the research of nonlinear optical signal processing for dense wavelength-division multiplexing optical transmission systems. Since 2019, he has been with Fujitsu Ltd. He is a Member of IEEE Photonics Society. He served on the Technical Program Committees of the OptoElectronics and Communications Conference and European Conference on Optical Communication.

**Yu Tanaka** (Member, IEEE) received the Ph.D. degree in material science from the Tokyo Institute of Technology, Tokyo, Japan, in 2000. In 2002, he joined Fujitsu Laboratories Ltd., Atsugi, Japan. Since then, he has been involved in the development of optical devices including quantum dot lasers and crystal-based photonic switches. In 2012, he joined the Photonics Electronics Technology Research Association, where he is currently a Senior Researcher. He is currently engaged in the development and industrialization of integrated silicon-photonics-based optical transceivers. He is a Member of the Institute of Electronics, Information, and Communications Engineers, Tokyo.

**Takeshi Hoshida** (Senior Member, IEEE) received the B.E., M.E., and Ph.D. degrees in electronic engineering from The University of Tokyo, Tokyo, Japan, in 1993, 1995, and 1998, respectively. In 1998, he joined Fujitsu Laboratories Ltd., Kawasaki, Japan, since then he has been engaged in the research and development of dense WDM optical transmission systems. From 2000 to 2002, he was with Fujitsu Network Communications, Inc., Richardson, TX, USA. Since 2007, he has been with Fujitsu Ltd., Kawasaki, and he currently heads Fujitsu's optical transmission research efforts. He is a Senior Member of the Institute of Electronics, Information and Communication Engineers and a Member of the Japan Society of Applied Physics. He was the recipient of the Commendation for Science and Technology by the Ministry of Education, Culture, Sports, Science and Technology (Awards for Science and Technology in Development Category) in 2020 and Japan Patent Office Commissioner Award of the National Commendation for Invention in 2020.